DOI: 10.1002/asia.200600083

Amine-Templated One-Dimensional Metal Sulfates Including a Mixed-Valent Fe Compound with a Half-Kagome Structure

J. N. Behera[a, b] and C. N. R. Rao*[a, b]

Abstract: Organically templated metal sulfates are relatively new. Six amine-templated transition-metal sulfates with different types of chain structures, including a novel iron sulfate with a chain structure corresponding to one half of the kagome structure, were synthesized by hydro/solvothermal methods. Amongst the one-dimensional metal sulfates, $[C_{10}N_2H_{10}][Zn(SO_4)Cl_2]$ (**1**) is the simplest, being formed by corner-linked ZnO_2Cl_2 and SO_4 tetrahedra. $[C_6N_2H_{18}][Mn(SO_4)_2(H_2O)_2]$ (**2**) and $[C_2N_2H_{10}][Ni(SO_4)_2(H_2O)_2]$ (**3**) have ladder structures comprising four-membered rings formed by SO_4 tetrahedra and metal–oxygen octahedra, just as in the mineral kröhnkite. $[C_4N_2H_{12}][V^{III}(OH)(SO_4)_2]\cdot H_2O$ (**4**) and $[C_4N_2H_{12}][VF_3(SO_4)]$ (**5**) exhibit chain topologies of the minerals tancoite and butlerite, respectively. The structure of $[C_4N_2H_{12}][H_3O][Fe^{III}Fe^{II}F_6(SO_4)]$ (**6**) is noteworthy in that it corresponds to half of the hexagonal kagome structure. It exhibits ferrimagnetic properties at low temperatures and the absence of frustration, unlike the mixed-valent iron sulfate with the full kagome structure.

Keywords: crystal engineering · half-kagome structures · iron · metal sulfates · one-dimensional chains

Introduction

Although a large number of metal silicates,[1] phosphates,[2] and carboxylates[3] with open-framework architectures have been synthesized and characterized over the years, open-framework metal sulfates are relatively new. In the last few years, a few open-framework materials involving oxyanions of Group 16 elements such as sulfate,[4] selenite,[5] and selenate[6] have been reported. An interesting aspect of the metal phosphates and carboxylates is the occurrence of materials with different dimensions. A few organically templated metal sulfates with different dimensional structures have also been described recently.[7] These results suggest that the sulfate ion can be used effectively to design open-framework and hybrid materials. The objective of the present study was to prepare metal sulfates with one-dimensional chain structures templated by organic amines. We have, indeed, succeeded in preparing and characterizing five amine-templated metal sulfates of composition $[C_{10}N_2H_{10}][Zn(SO_4)Cl_2]$ (**1**), $[C_6N_2H_{18}][Mn(SO_4)_2(H_2O)_2]$ (**2**), $[C_2N_2H_{10}][Ni(SO_4)_2(H_2O)_2]$ (**3**), $[C_4N_2H_{12}][V^{III}(OH)(SO_4)_2]\cdot H_2O$ (**4**), and $[C_4N_2H_{12}][VF_3(SO_4)]$ (**5**), all of which have chain structures comparable to those in some of the minerals. Of these, **1** has the simplest possible chain structure formed by SO_4 and ZnO_2Cl_2 tetrahedra. What is more significant, however, is that we were able to prepare an amine-templated mixed-valent iron sulfate with the formula $[C_4N_2H_{12}][H_3O][Fe^{III}Fe^{II}F_6(SO_4)]$ (**6**), which corresponds to half of the hexagonal kagome structure with Fe in two oxidation states. Such a compound is of significance in view of the great interest in the synthesis and magnetic properties of compounds with the hexagonal kagome-type layers.[8] Interestingly, the half-kagome structure exhibits magnetic properties that are different from those of a regular kagome structure containing mixed-valent iron.

[a] J. N. Behera, Prof. Dr. C. N. R. Rao
Solid State and Structural Chemistry Unit
Indian Institute of Science
Bangalore 560012 (India)
Fax: (+91) 802-208-2760
E-mail: cnrrao@jncasr.ac.in

[b] J. N. Behera, Prof. Dr. C. N. R. Rao
Chemistry and Physics of Materials Unit
Jawaharlal Nehru Centre for
Advanced Scientific Research
Jakkur P.O., Bangalore 560064 (India)

Results and Discussion

We first describe the structures of the five amine-templated metal sulfates with chain structures akin to those of the minerals chalcanthite, kröhnkite, tancoite, and butlerite.

$[C_{10}N_2H_{10}][Zn(SO_4)Cl_2]$ (1)

The asymmetric unit of **1** consists of 20 non-hydrogen atoms, six of which belong to the inorganic framework and 14 to 4,4-bipyridine (bpy). There is one crystallographically distinct Zn atom and one S atom, with the Zn atom in a tetrahedral coordination. Two unidentate SO_4^{2-} groups and two Cl atoms tetrahedrally coordinate the Zn atom. The Zn–Cl bond lengths of 2.221(2) and 2.221(3) Å are considerably longer than the Zn–O(sulfate) bond lengths of 1.978(4) and 1.993(4) Å. The sulfate is a regular tetrahedron and acts as a bidentate bridging metal linker. All the O–S–O angles and S–O bond lengths are in the normal range. Selected bond lengths and angles of **1** are listed in Table 1.

The extended structure of **1** consists of parallel inorganic chains templated by bpy; the individual chains contain corner-sharing ZnO_2Cl_2 and SO_4 tetrahedra. Each sulfate ligand uses two oxygen atoms to link two zinc centers and bridges two ZnO_2Cl_2 tetrahedra, each of which, in turn, share their vertices with two SO_4 groups. This generates a simple –Zn–O–S–O–Zn– [T–T] wirelike chain along the *a* axis (Figure 1 a). Adjacent chains interact through hydrogen bonds involving the terminal S=O and Zn–Cl bonds as well as bpy to form a three-dimensional assembly (Figure 1 b). A similar single-stranded structure of zinc sulfate in which zinc is in octahedral coordination was reported recently.[9] The $[M(TO_4)\phi_2]$ chain backbone observed in **1** is the simplest possible [T–T] 1D structure. Notably, the mineral chalcanthite[10] has an O–T chain structure. It is interesting that bpy is in the interchain region with the protonated nitrogen atom in **1** instead of coordinating to the metal.

Table 1. Selected bond lengths and angles in **1**.[a]

Moiety	Bond length [Å]	Moiety	Angle [°]
Zn(1)–O(1)	1.978(4)	O(1)–Zn(1)–O(2)	99.3(2)
Zn(1)–O(2)	1.993(4)	O(1)–Zn(1)–Cl(1)	112.6(2)
Zn(1)–Cl(1)	2.221(2)	O(2)–Zn(1)–Cl(1)	111.6(2)
Zn(1)–Cl(2)	2.227(3)	O(1)–Zn(1)–Cl(2)	102.3(2)
S(1)–O(3)	1.449(4)	O(2)–Zn(1)–Cl(2)	111.16(14)
S(1)–O(4)	1.451(4)	Cl(1)–Zn(1)–Cl(2)	117.97(8)
S(1)–O(1)	1.466(4)	O(3)–S(1)–O(4)	109.5(3)
S(1)–O(2)	1.483(4)	O(3)–S(1)–O(1)#1	110.7(3)
N(1)–C(5)	1.305(9)	O(4)–S(1)–O(1)#1	110.2(3)
N(1)–C(1)	1.309(10)	O(3)–S(1)–O(2)	111.3(3)
C(1)–C(2)	1.354(10)	O(4)–S(1)–O(2)	107.6(3)
C(2)–C(3)	1.370(9)	O(1)#1–S(1)–O(2)	107.5(3)
C(3)–C(4)	1.372(9)	S(1)#2–O(1)–Zn(1)	129.4(3)
C(3)–C(3)#3	1.474(12)	S(1)–O(2)–Zn(1)	126.5(2)
C(4)–C(5)	1.349(10)	C(5)–N(1)–C(1)	121.3(7)
N(2)–C(10)	1.312(7)	N(1)–C(1)–C(2)	120.4(8)
N(2)–C(6)	1.322(8)	C(1)–C(2)–C(3)	120.9(8)
C(6)–C(7)	1.379(8)	C(2)–C(3)–C(4)	115.7(6)
C(7)–C(8)	1.374(8)	C(2)–C(3)–C(3)#3	122.0(8)
C(8)–C(9)	1.373(8)	C(4)–C(3)–C(3)#3	122.3(8)
C(8)–C(8)#4	1.506(11)	C(5)–C(4)–C(3)	121.5(7)
C(9)–C(10)	1.380(8)	N(1)–C(5)–C(4)	120.1(7)
		C(10)–N(2)–C(6)	121.8(6)
		N(2)–C(6)–C(7)	120.1(6)
		C(8)–C(7)–C(6)	120.1(6)
		C(9)–C(8)–C(7)	117.7(5)
		C(9)–C(8)–C(8)#4	121.3(6)
		C(7)–C(8)–C(8)#4	121.1(6)
		C(8)–C(9)–C(10)	120.2(6)
		N(2)–C(10)–C(9)	120.2(6)

[a] Symmetry transformations used to generate equivalent atoms: #1: $x+1, y, z$; #2: $x-1, y, z$; #3: $-x+2, -y, -z$; #4: $-x+2, -y, -z+1$.

$[C_6N_2H_{18}][Mn(SO_4)_2(H_2O)_2]$ (2) and $[C_2N_2H_{10}][Ni(SO_4)_2(H_2O)_2]$ (3)

The inorganic framework structures of **2** and **3** are similar; both have the topology of the mineral kröhnkite, $[Na_2Cu^{II}(SO_4)_2]\cdot 2H_2O$.[10] The only difference between the structures of **2** and **3** is in the templated amine (Figure 2). Compound **2** is a one-dimensional manganese sulfate templated by hexamethylenediamine (hmda), whereas **3** is a one-dimensional nickel sulfate templated by ethylenediamine (en). The asymmetric unit of **2** consists of 11 non-hydrogen atoms, seven of which belong to the inorganic framework and four to the amine molecules, whereas that of **3** consists of nine non-hy-

Abstract in Kannada:

ಆಂಶಾಂತಿಯಾಗಿ ತಯಾರಿಸಿದ ಸಲ್ಫೇಟುಗಳ ಪಡಿಯಚ್ಚು ಸುಮಾರಾಗಿ ನೂತನವಾದುದು. ಕಗೊಮೆ ವಿನ್ಯಾಸದ ಅರ್ಧ ಭಾಗಕ್ಕೆ ಸರಿಹೊಂದುವ ಸರಳ ವಿನ್ಯಾಸವುಳ್ಳ ಕಬ್ಬಿಣದ ಸಲ್ಫೇಟನ್ನೂ ಒಳಗೊಂಡಂತೆ ವಿಭಿನ್ನ ರೀತಿಗಳ ಸರಳ ವಿನ್ಯಾಸದ ಆರು ಅಮೀನುಗಳುಳ್ಳ ಸಂಕ್ರಮಣ ಲೋಹಗಳ ಪಡಿಯಚ್ಚುಗಳನ್ನು ಹೈಡ್ರೋ/ಸಾಲ್ವೋ ಥರ್ಮಲ್ ವಿಧಾನಗಳ ಮೂಲಕ ತಯಾರಿಸಲಾಯಿತು. ಏಕವಿಮೀತಿಯ ಲೋಹ ಸಲ್ಫೇಟುಗಳಲ್ಲಿ ಮೂಲೆಗಳಲ್ಲಿ ಜೊತೆಗೊಂಡ $[ZnO_2Cl_2]$ ಮತ್ತು ನಾಲ್ಕುಪಕ್ಕಗಳಿರುವ ಘನ SO_4 ಗಳಿಂದ ರಚನೆಯಾದ $[C_{10}N_2H_{10}][Zn(SO_4)Cl_2]$ (1) ಅತ್ಯಂತ ಸರಳವಾದುದು. $[C_6N_2H_{18}][Mn(SO_4)_2(H_2O_2)]$ (2) ಮತ್ತು $[C_2N_2H_{10}][Ni(SO_4)_2(H_2O_2)]$ (3)ಗಳಿಗೆ ನಾಲ್ಕುಪಕ್ಕಗಳಿರುವ ಘನ SO_4 ಮತ್ತು ಕ್ರಾಂಷ್ನೈಕಲ ಟ್ ಖನಿಜದಲ್ಲಿರುವಂತೆ ಎಂಟುಪಕ್ಕಗಳಿರುವ ಲೋಹ-ಆಕ್ಸಿಜನ್ ಗಳಿಂದ ರಚಿಸಿದ ಏಣಿ ವಿನ್ಯಾಸವಿರುತ್ತವೆ.

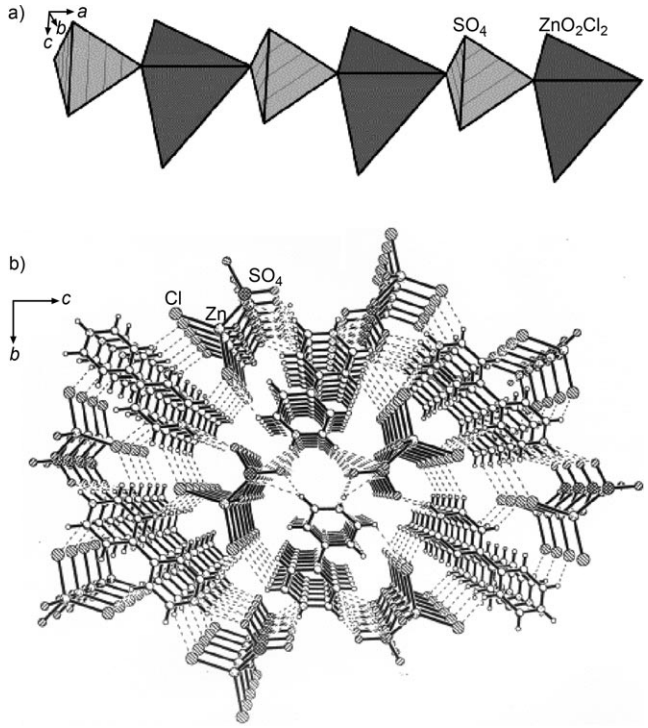

Figure 1. a) Polyhedral view of the inorganic part of $[C_{10}N_2H_{10}][Zn(SO_4)Cl_2]$ (**1**) along the *a* axis. b) 3D assembly formed by the chains and the amine molecules in **1**, creating the channels.

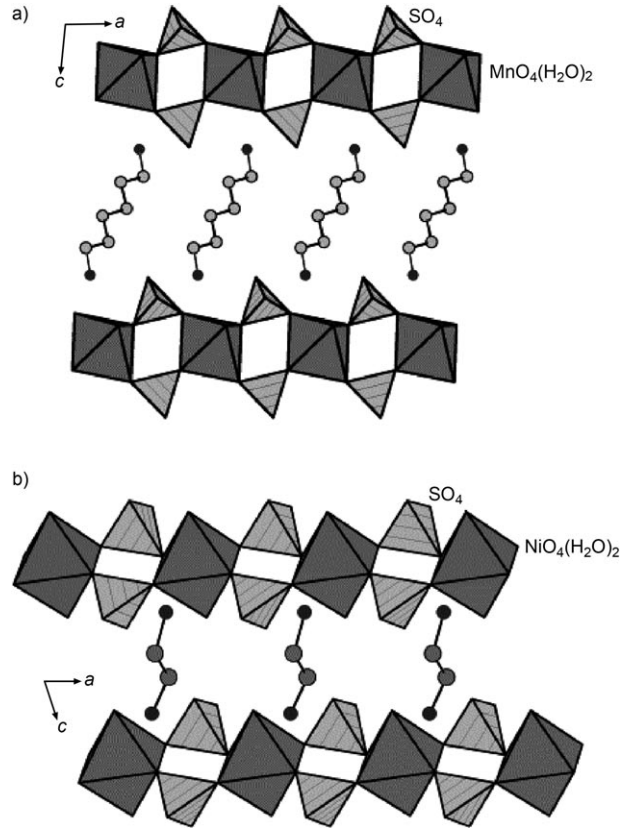

Figure 2. Polyhedral view of a) $[C_6N_2H_{18}][Mn(SO_4)_2(H_2O)_2]$ (**2**) and b) $[C_2N_2H_{10}][Ni(SO_4)_2(H_2O)_2]$ (**3**) showing the chain of corner-sharing four-membered rings. Amine molecules are present in the interchain space.

drogen atoms, of which seven belong to the framework and two to the amine part. There is one crystallographically distinct metal atom and one S atom, with the metal atom in octahedral geometry. The octahedral coordination around the metal atom is defined by four μ-O groups from four sulfate and two aqua ligands. The sulfate ion is distorted and shares two corners with two adjacent metal octahedra, leaving two terminal S=O bonds. The bonds to the coordinating oxygen atoms are significantly longer than the S=O bonds. Selected bond lengths and angles of **2** are listed in Table 2.

Table 2. Selected bond lengths and angles in **2**.[a]

Moiety	Bond length [Å]	Moiety	Angle [°]
Mn–O(4)	2.149(3)	O(4)–Mn–O(4)#1	180.000(2)
Mn–O(1)#2	2.187(3)	O(4)–Mn–O(1)#2	93.73(11)
Mn–O(3)	2.208(3)	O(4)#1–Mn–O(1)#2	86.27(11)
S–O(5)	1.452(3)	O(1)#2–Mn–O(1)#3	179.999(2)
S–O(2)	1.462(3)	O(4)–Mn–O(3)	89.60(14)
S–O(4)	1.469(3)	O(4)#1–Mn–O(3)	90.40(14)
S–O(1)	1.480(3)	O(1)#2–Mn–O(3)	89.45(12)
N(1)–C(1)	1.474(6)	O(1)#3–Mn–O(3)	90.55(12)
C(1)–C(2)	1.510(7)	O(4)–Mn–O(3)#1	90.40(14)
C(2)–C(3)	1.516(7)	O(3)–Mn–O(3)	179.999(1)
		O(5)–S–O(2)	111.7(2)
		O(5)–S–O(4)	110.2(2)
		O(2)–S–O(4)	106.4(2)
		O(5)–S–O(1)	109.5(2)
		O(2)–S–O(1)	109.4(2)
		O(4)–S–O(1)	109.5(2)
		S–O(1)–Mn	135.3(2)
		S–O(4)–Mn	136.8(2)
		N(1)–C(1)–C(2)	111.5(4)
		C(1)–C(2)–C(3)	112.3(4)
		C(2)–C(3)–C(3)#5	113.8(5)

[a] Symmetry transformations used to generate equivalent atoms: #1: −x, −y+2, −z+2; #2: −x−1, −y+2, −z+2; #3: x+1, y, z; #4: x−1, y, z; #5: −x, −y+2, −z+1.

In both **2** and **3**, a pair of sulfate tetrahedra share corners to form a one-dimensional chain structure with four-membered rings by bridging the neighboring metal octahedra. The chain is formed of alternating $[M^{2+}O_4(H_2O)_2]$ octahedra and pairs of SO_4 teterahedra, with the H_2O groups in a *trans* arrangement around the divalent cation. The diammonium cations are located between the chains; they form hydrogen bonds with framework oxygen atoms that govern the stability of the structure. Several naturally occurring minerals as well as synthetic compounds with related structures are known.[11] Fleck et al.[12] recently reviewed compounds with the kröhnkite-type topology and attempted to provide a structural classification. The minerals collinsite, $Ca_2[Mg(PO_4)(H_2O)_2]$, and fairfieldite, $Ca_2[Mn(PO_4)_2(H_2O)_2]$, based on the general $[M(TO_4)_2\phi_2]$ chain, are part of the kröhnkite family. The common occurrence of the kröhnkite-type chain involving of PO_4^{3-}, AsO_4^{3-}, SO_4^{2-}, and SeO_4^{2-} anions is probably because the corner link between MO_6 and TO_4 groups is flexible, involving no steric constraints.

CHEMISTRY
AN ASIAN JOURNAL

$[C_4N_2H_{12}][V^{III}(OH)(SO_4)_2]\cdot H_2O$ (4)

The asymmetric unit of **4** consists of 19 non-hydrogen atoms with one crystallographically distinct V and two S atoms. The V atom makes four V–O–S and two V–(OH)–V linkages to the neighboring S and V atoms, respectively. The S atoms form two S–O–V bonds with each of the adjacent vanadium atoms, the remaining two being terminal S=O bonds. The framework structure is built up of infinite chains of $[V^{III}(OH)(SO_4)_2]_n^{2-}$ running along the *c* axis. The $VO_4(OH)_2$ octahedra in **4** share vertices in a *trans* fashion through the (OH) groups, and the SO_4 tetrahedra are grafted onto the chain to form the tancoite-type topology (Figure 3). The 1D chains are arranged parallel to one another, with the diprotonated amine and water molecules residing in the interchain space and forming strong hydrogen bonds with the framework. Compound **4** is isostructural to $[C_2N_2H_{10}][V^{III}(OH)(SO_4)_2]\ H_2O$,[4b] templated by ethylenediamine. The use of dabco as the templating amine has been reported to give rise to the same type of chain[4b] with the $VO_4(OH)_2$ octahedra sharing their vertices in an alternating *cis–trans* fashion. It is not clear why a large number of vanadium sulfates occur with chain structures. To our knowledge, no organically templated two- or three-dimensional vanadium sulfate has been reported hitherto, unlike the two- and three-dimensional vanadium phosphates.[13]

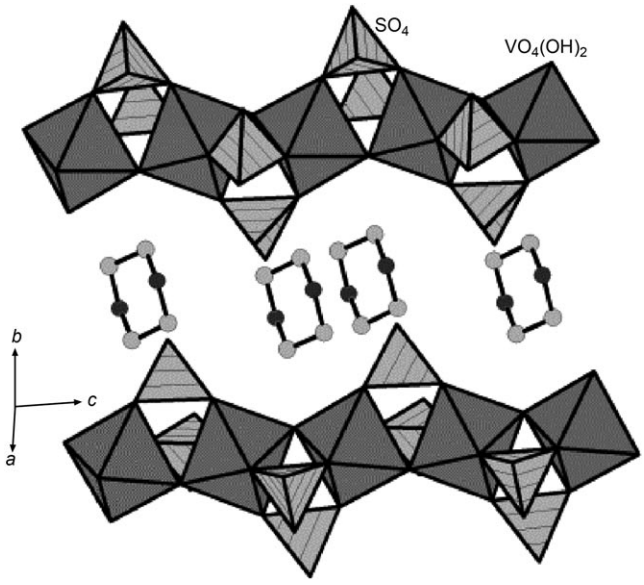

Figure 3. Polyhedral view of $[C_4N_2H_{12}][V^{III}(OH)(SO_4)_2]\ H_2O$ (**4**) along the *b* axis with the symmetrical bridging of the sulfate tetrahedra. Note the tancoite-type chains in **4**.

$[H_2N(CH_2)_4NH_2][VF_3(SO_4)]$ (5)

The asymmetric unit of **5** consists of 16 non-hydrogen atoms, of which 10 belong to the inorganic framework and six to the organic guest molecules. There are two crystallographically distinct V atoms with octahedral geometry. The V–O bond lengths in **4** are in the range 1.997(5)–2.028(5) Å with an average of 2.012 Å. The V–F bond lengths are in the range 1.878(4)–1.963(4) Å with an average of 1.909 Å. The *cis*-O/F–V–O/F bond angles are between 87.0(2) and 93.0(2)° ((*cis*-O/F–V(1)–O/F)$_{av}$ = 90.0° and (*cis*-O/F–V(2)–O/F)$_{av}$ = 90.0°) and the *trans*-O/F–V–O/F bond angle is 180°, indicating near-perfect octahedral geometry for **5**.

The structure of $[C_4N_2H_{12}][VF_3(SO_4)]$ consists of VF_4O_2 octahedra sharing vertices with the neighbors through the fluorine atoms (Figure 4a). The sulfate tetrahedra are bridged onto the *trans* vertices of the metal octahedra along the chain. The *trans* orientation of the bridging F atom creates a zigzag {–F–V–F–V–} backbone to the linear chain of VF_4O_2 octahedra, forming an analogue of the butlerite-type chain.[14] In the sulfate tetrahedra, two oxygens bond to the adjacent V sites of the vertex-shared VF_4O_2 octahedra in a symmetrical bridge, and the remaining two form terminal S=O bonds. The individual chains are held together by hydrogen-bond interactions involving diprotonated amine molecules. The 1D chain in **5** also interacts with the amine molecules through hydrogen bonding to form cavities. Bond valence sum (BVS) calculations using the method of Brown and Altermatt[15] (V(1) = 3.15, V(2) = 3.20) indicate that the valence state of V is +3 and confirm the position of the fluorine atom (F(1) = 0.62, F(2) = 0.99, F(3) = 0.60). The

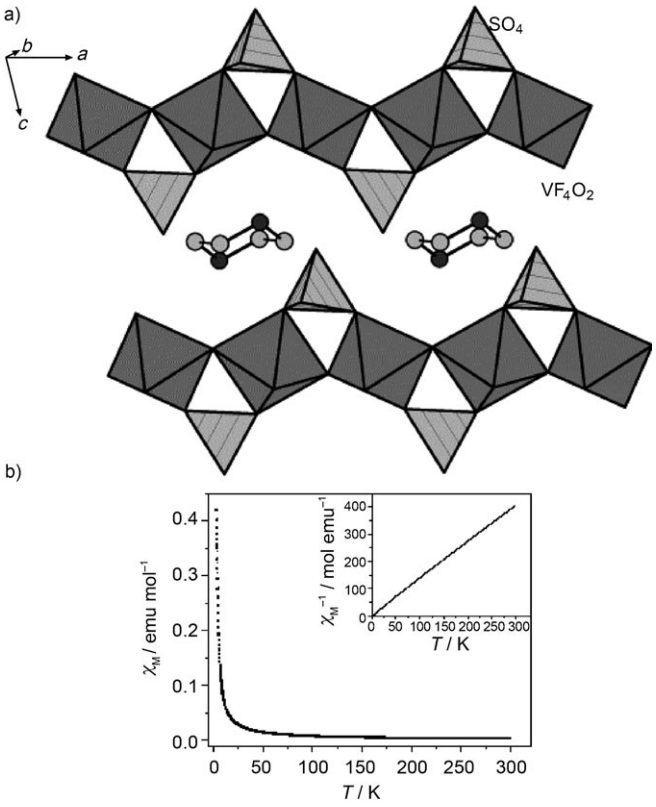

Figure 4. a) Polyhedral view of $[C_4N_2H_{12}][VF_3(SO_4)]$ (**5**) along the *b* axis with alternating up–down bridging of the sulfate tetrahedron. Note the butlerite-type chains. b) Temperature variation of the magnetic susceptibility of **5**. The inset shows the variation of inverse susceptibility.

chain structure in **5** is isostructural to $[C_4N_2H_{12}][Fe^{III}F_3(SO_4)]$[4c] and is comparable to the chain of *cis* corner-sharing octahedra in fiboferrite, $[Fe^{3+}(OH)(H_2O)_2(SO_4)]\cdot(H_2O)_3$, with a helical configuration. In fibroferite as well as butlerite, $[Fe^{3+}(OH)(H_2O)_2(SO_4)]$, and parabutlerite, $[Fe^{3+}(OH)(H_2O)(SO_4)]$, the chains are linked solely by hydrogen bonds, as there are no interstitial cations, whereas in organically templated compounds, the chains are held together by the hydrogen-bond assembly of the diprotonated amine molecules located in the interchain space to form the 3D assembly.

The variable-temperature magnetic-susceptibility data of **5** at 5000 Oe are shown in Figure 4b. The compound is predominantly paramagnetic, and the inverse susceptibility data (inset of Figure 4b) show a linear behavior in the temperature range 50–300 K, yielding a small negative Weiss temperature of −5 K which indicates weak antiferrimagnetic interaction. The effective magnetic moment per vanadium atom calculated from the fit of the χ_M^{-1} versus T curve is 2.4 μ_B, which is slightly lower than expected for V^{III} centers (theoretical $\mu_{eff}=2.8$ μ_B).

$[C_4N_2H_{12}][H_3O][Fe^{III}Fe^{II}F_6(SO_4)]$ (6) with a Half-Kagome Structure

The asymmetric unit of **6** consists of 21 non-hydrogen atoms, 14 of which belong to the inorganic framework with three crystallographically distinct Fe atoms and one S atom and 7 belong to the extraframework guest molecules; one extraframework oxygen atom belongs to the hydronium ion. Two Fe atoms (Fe(2) and Fe(3)) are in special positions (occupancy = 0.5). The structure of **6** consists of anionic chains of vertex-sharing $Fe^{III}F_5O$, $Fe^{II}F_4O_2$ octahedra and sulfate tetrahedral units, which are fused together by $Fe^{III/II}$–F–$Fe^{III/II}$ and $Fe^{III/II}$–O–S bonds. The Fe–O bond lengths in **6** are in the range 2.054(5)–2.139(5) Å and the Fe–F bond lengths are 1.903(4)–2.111(4) Å ($(Fe(1)^{III}–F)_{av}=1.92$ Å, $Fe(2)^{II}–F)_{av}=2.05$ Å, $Fe(3)^{II}–F)_{av}=2.06$ Å). The bond lengths and angles indicate perfect octahedral geometry around Fe centers. BVS calculations[15] using r_0(Fe–F) = 1.679 and r_0(Fe–O) = 1.759 Å gave valence sums Fe(1) = 3.03, Fe(2) = 2.12, Fe(3) = 2.09. The average Fe–O/F bond lengths also indicate the oxidation state of Fe(1) to be +3, and the remaining two Fe centers to be +2. The position of the fluorine atoms find indirect support from BVS calculations (F(1) = 0.54, F(2) = 0.51, F(3) = 0.84, F(4) = 0.50, F(5) = 0.82, F(6) = 0.80). Thus, the framework stoichiometry of $[Fe^{III}Fe^{II}F_6(SO_4)]$ with a −3 charge requires the amine to be doubly protonated, in addition to the presence of the hydronium ion. The Mössbauer spectrum at room temperature confirms the presence of two types of Fe^{II} and one Fe^{III} species in **6**. Selected bond lengths and angles of **6** are listed in Table 3.

The fluorine and the oxygen neighbors in **6** are coordinated octahedrally to the Fe atoms ($Fe(1)^{III}F_5O$, $Fe(2)^{II}F_4O_2$, $Fe(3)^{II}F_4O_2$). The $Fe(2)^{II}F_4O_2$ and $Fe(3)^{I}F_4O_2$ octahedra are vertex-shared through *trans* Fe(2)–F(6)–Fe(3) linkages, which run along the *a* axis of the unit cell. Each of the octahedra shares four of its Fe–F vertices with similar neighbors. $Fe(1)^{III}F_5O$ octahedra share one Fe–F vertex each with $Fe(2)^{II}$ and $Fe(3)^{II}$ octahedra in an up and down manner. Such connectivity creates a triangular lattice formed by $Fe(1)^{III}F_5O$, $Fe(2)^{II}F_4O_2$, and $Fe(3)^{II}F_4O_2$ octahedra (Figure 5a). The sulfate tetrahedron caps the triangular lattice in a manner similar to that in jarosites with the kagome lattice, in which Fe is in the +3 oxidation state.[16] The structure can be described as half-kagome, as two such chains can produce the complete one. In the full kagome structure, each octahedron shares four of its M–F vertices with similar neighbors with the M–F–M bonds roughly aligned in the *ab* plane. The presence of three Fe(1)–F terminal bonds in **6** could be responsible for not forming the complete kagome structure. The individual chains are held together by strong hydrogen-bond interactions (N–H···O, N–H···F, C–H···O, and C–H···F) by the framework oxygen and fluorine atoms with protonated water and diprotonated amine molecules to

Table 3. Selected bond lengths and angles in **6**.[a]

Moiety	Bond length [Å]	Moiety	Bond length [Å]
Fe(1)–F(1)	1.903(4)	S(1)–O(3)	1.447(5)
Fe(1)–F(3)	1.924(4)	S(1)–O(4)	1.477(5)
Fe(1)–F(2)	1.925(4)	S(1)–O(2)	1.478(5)
Fe(1)–F(4)	1.926(4)	S(1)–O(1)	1.479(5)
Fe(1)–F(5)	1.931(4)	N(1)–C(2)	1.447(11)
Fe(1)–O(1)	2.054(5)	N(1)–C(4)	1.499(12)
Fe(2)–F(6)	2.023(4)	C(1)–C(2)	1.445(11)
Fe(2)–F(3)	2.085(4)	C(1)–N(2)	1.504(12)
Fe(2)–O(2)	2.132(5)	C(3)–C(4)	1.433(11)
Fe(3)–F(6)	2.014(4)	C(3)–N(2)	1.498(11)
Fe(3)–F(4)	2.111(4)		
Fe(3)–O(4)	2.140(5)		

Moiety	Angle [°]	Moiety	Angle [°]
F(1)–Fe(1)–F(3)	92.0(2)	F(6)–Fe(3)–F(4)	91.6(2)
F(1)–Fe(1)–F(2)	89.6(2)	F(6)#2–Fe(3)–F(4)	88.4(2)
F(3)–Fe(1)–F(2)	89.6(2)	F(4)–Fe(3)–F(4)#2	180.000(1)
F(1)–Fe(1)–F(4)	90.6(2)	F(6)–Fe(3)–O(4)	95.4(2)
F(3)–Fe(1)–F(4)	89.4(2)	F(6)#2–Fe(3)–O(4)	84.6(2)
F(2)–Fe(1)–F(4)	178.9(2)	F(4)–Fe(3)–O(4)	92.8(2)
F(1)–Fe(1)–F(5)	92.2(2)	O(4)#2–Fe(3)–O(4)	180
F(3)–Fe(1)–F(5)	175.7(2)	O(3)–S(1)–O(4)	110.5(3)
F(2)–Fe(1)–F(5)	90.3(2)	O(3)–S(1)–O(2)	109.8(3)
F(4)–Fe(1)–F(5)	90.8(2)	O(4)–S(1)–O(2)	108.9(3)
F(1)–Fe(1)–O(1)	177.4(2)	O(3)–S(1)–O(1)	109.6(3)
F(3)–Fe(1)–O(1)	89.8(2)	O(4)–S(1)–O(1)	108.6(3)
F(2)–Fe(1)–O(1)	88.5(2)	O(2)–S(1)–O(1)	109.5(3)
F(4)–Fe(1)–O(1)	91.3(2)	Fe(1)–F(3)–Fe(2)	135.0(2)
F(5)–Fe(1)–O(1)	85.9(2)	Fe(1)–F(4)–Fe(3)	132.3(2)
F(6)–Fe(2)–F(6)#1	180	S(1)–O(1)–Fe(1)	136.3(3)
F(6)–Fe(2)–F(3)	91.6(2)	Fe(3)–F(6)–Fe(2)	127.1(2)
F(6)–Fe(2)–F(3)	88.4(2)	S(1)–O(2)–Fe(2)	127.6(3)
F(3)–Fe(2)–F(3)#1	180	S(1)–O(4)–Fe(3)	126.9(3)
F(3)–Fe(2)–O(2)	88.9(2)	C(2)–N(1)–C(4)	111.2(7)
F(6)–Fe(2)–O(2)	94.9(2)	C(2)–C(1)–N(2)	113.1(7)
F(6)–Fe(2)–O(2)	85.1(2)	C(1)–C(2)–N(1)	114.1(7)
F(3)–Fe(2)–O(2)	91.1(2)	C(4)–C(3)–N(2)	112.4(7)
O(2)#1–Fe(2)–O(2)	179.999(1)	C(3)–C(4)–N(1)	112.2(7)
F(6)–Fe(3)–F(6)#2	180	C(3)–N(2)–C(1)	109.9(7)

[a] Symmetry transformations used to generate equivalent atoms: #1: $-x$, $-y+1$, $-z+2$; #2: $-x+1$, $-y+1$, $-z+2$.

CHEMISTRY
AN ASIAN JOURNAL

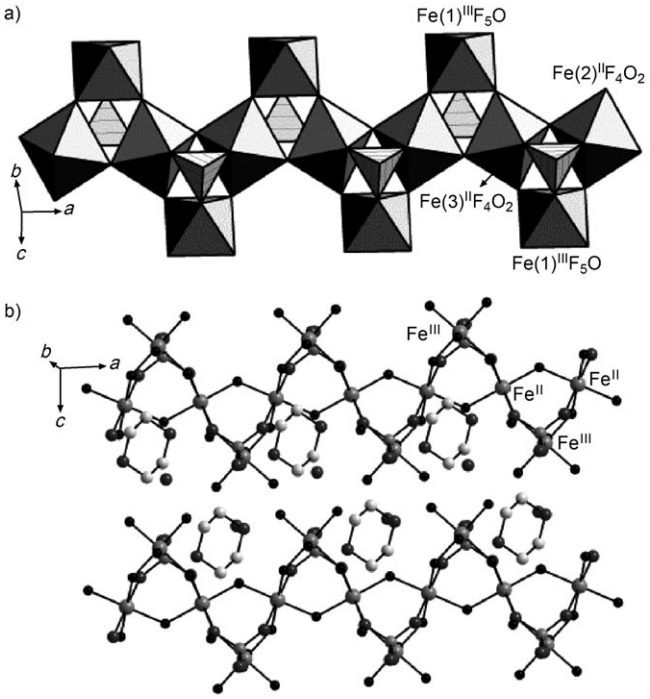

Figure 5. a) Polyhedral view of the inorganic chain of $[C_4N_2H_{12}][H_3O][Fe^{III}Fe^{II}F_6(SO_4)]$ (**6**) along the *a* axis. The three-membered apertures are capped by sulfate moieties. b) Ball and stick view of **6** in the *ac* plane. Diprotonated amine and protonated water molecules occupy positions in-between the chains.

Table 4. Hydrogen-bonding interactions in compounds **1**, **2**, and **6**.

D–H···A	D–H [Å]	H···A [Å]	D···A [Å]	D–H···A [°]
		1		
N(1)–H(1)···O(3)	0.861(10)	1.906(9)	2.700(9)	152.8(8)
N(2)–H(6)···O(4)	0.860(7)	1.818(7)	2.677(7)	178.7(6)
C(1)–H(2)···Cl(1)	0.928(13)	2.738(10)	3.575(10)	150.4(10)
C(2)–H(3)···Cl(1)	0.930(12)	2.698(9)	3.531(10)	149.5(9)
C(5)–H(5)···Cl(2)	0.929(10)	2.743(9)	3.461(9)	134.8(8)
C(6)–H(7)···O(2)	0.929(10)	2.545(8)	3.385(9)	150.4(7)
C(6)–H(7)···O(4)	0.929(10)	2.443(8)	3.265(9)	147.4(7)
C(10)–H(10)···Cl(2)	0.929(10)	2.783(7)	3.413(9)	126.0(6)
		2		
N(1)–H(1)···O(3)	0.83(5)	2.48(5)	3.093(6)	132(4)
N(1)–H(1)···O(5)	0.83(5)	2.19(5)	2.782(6)	128(4)
N(1)–H(2)···O(2)	0.95(8)	2.16(9)	3.048(6)	156(7)
N(1)–H(2)···O(4)	0.95(8)	2.15(8)	2.900(5)	135(7)
N(1)–H(3)···O(2)	0.87(7)	1.99(7)	2.854(6)	171(6)
O(3)–H(10)···O(1)	0.91(7)	2.03(7)	2.825(4)	146(6)
Intra O(3)–H(11)···O(5)	0.83(7)	1.86(8)	2.649(5)	159(7)
C(1)–H(4)···O(5)	0.99(6)	2.56(5)	3.099(6)	114(4)
		6		
N(1)–H(1)···F(5)	0.920(13)	2.510(10)	3.19(10)	131.1(10)
N(1)–H(2)···O(2)	0.920(13)	2.568(11)	3.337(11)	141.4(10)
N(2)–H(11)···F(4)	0.920(13)	2.516(10)	3.355(10)	151.9(10)
N(2)–H(12)···F(3)	0.920(13)	2.411(10)	3.119(10)	133.8(9)
O(50)–H(13)···F(6)	1.08(5)	1.73(4)	2.787(8)	166(8)
O(50)–H(14)···F(5)	1.17(6)	1.66(7)	2.800(9)	164(7)
O(50)–H(15)···F(2)	1.2(2)	2.2(4)	2.792(9)	107(24)
O(50)–H(15)···F(2)	1.2(2)	2.4(4)	3.313(8)	129(26)
O(50)–H(15)···O(1)	1.2(2)	2.3(3)	2.913(8)	107(15)
C(1)–H(3)···O(2)	0.990(13)	2.452(10)	3.294(11)	142.6(8)
C(1)–H(4)···F(1)	0.991(13)	2.429(9)	3.210(9)	135.3(9)
C(2)–H(5)···F(1)	0.991(11)	1.694(9)	2.684(9)	177.6(8)
C(2)–H(6)···O(4)	0.990(11)	2.001(9)	2.791(9)	135.1(8)
C(3)–H(7)···F(2)	0.990(11)	1.892(9)	2.816(9)	154.0(8)
C(3)–H(8)···O(3)	0.991(11)	1.925(9)	2.874(9)	159.5(8)
C(4)–H(10)···F(5)	0.990(13)	2.387(10)	3.327(10)	158.4(9)

stabilize the structure (Figure 5b). The various hydrogen-bond interactions for **1**, **2**, and **6** are given in Table 4.

In Figure 6a, we show the variable-temperature magnetic susceptibility (χ) data of **6** recorded at 100 Oe under zero-field-cooled (ZFC) and field-cooled (FC) conditions. From this figure, we see that although there are some differences between the ZFC and FC data, there is no clear indication of frustration as in the case of the mixed-valent iron kagome structure reported in the literature.[17] In the inset of Figure 6a, we show the variation of inverse susceptibility with temperature. In the paramagnetic region, the susceptibility follows the Curie–Weiss law with a Weiss temperature of -90 K as obtained from the fit of the χ_M^{-1} data in the 100–300 K range. The negative θ_p value suggests that the exchange interaction is antiferrimagnetic. The effective magnetic moment of Fe is 5.2 μ_B, slightly lower than the expected spin-only value of 5.4 μ_B, which lies between typical values for high-spin Fe^{II} and Fe^{III}, confirming the mixed-valent state of iron.

In Figure 6b we show the variation of χT with temperature. The behavior is reminiscent of a ferrimagnetic system. Accordingly, the χT data at low temperatures do not obey the Curie law. As the system consists of Fe^{2+} and Fe^{3+} ions arranged in a sawtooth lattice with almost equal exchange coupling, the three Fe–F–Fe angles being nearly the same ($\approx$130°), the low-energy spectrum is expected to be irregular in total spin or magnetization. Notably, this is a J_1, J_2 system with alternate J_2 missing. The ground state of **6** appears to involve fluctuations in the spin moment of each of the Fe ions, and the total magnetization of the ground state is 0.5 times the number of triangles. The lowest excited state would have a magnetization one unit lower than the ground-state spin value. Thereafter, within small energy intervals, the magnetization of the levels fluctuates, showing irregularities in terms of alternate lower and higher magnetizations values.[18] The sharp and well-rounded minimum in the χT plot at low temperatures is due to such irregular magnetization values in the low-energy spectrum. The minimum is due to states with magnetizations smaller than the ground-state magnetization becoming populated at low temperatures. Owing to the mixed-spin nature, the sawtooth lattice does not experience frustration. The low-temperature susceptibility is purely due to the low-energy spectrum of a typical ferrimagnetic system with competing interactions.[18] At the lowest temperatures, the χT value should be equal to the fluctuation in the ground-state magnetization. However, the susceptibility becomes small and nearly vanishes owing to higher dimensional coupling. We do not observe distinct magnetic hysteresis in **6** owing to weak interactions between

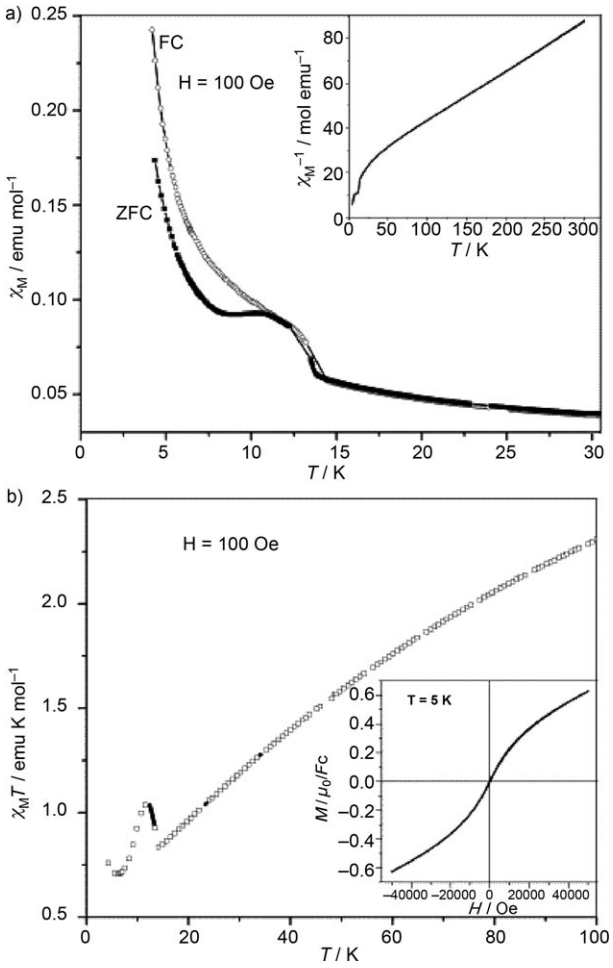

Figure 6. a) Temperature variation of the magnetic susceptibility of **6**. The inset shows the variation of inverse susceptibility. b) Variation of χT with temperature. The inset shows the *M–H* curve at 5 K.

the chains. However, nonlinear *M–H* behavior is observed, as shown in the inset of Figure 6b.

The half-kagome structure of **6** is different from the mixed-valent kagome compound reported earlier.[17] In the mixed-valent kagome compound, the frustration is prevalent as the magnetic triangles are strongly connected to the hexagonal structure through corner-shared octahedra. In addition, ferrimagnetic interactions are observed owing to the presence of the integral spin Fe^{2+} ($S=2$) in the system.[19] On the other hand, very weak interactions exist between the chains of the half-kagome compound, effects of which are seen only at very low temperatures. Notably, pure Fe^{3+} kagome structures show magnetic frustration or AFM ordering at low temperatures. Thus, Nocera et al.[20] found a pure Fe^{3+} jarosite to show AFM ordering at 61.4 K.

Conclusions

In summary, six organically templated transition-metal sulfates with 1D structures, with organic amines as templating agents, have been synthesized and characterized, establishing thereby the use of the sulfate group in building different architectures. The formation of chain structures similar to kröhnkite, butlerite, and tancoite in these compounds just as in the organically templated metal phosphates, suggests that it should be possible to obtain complex 2D and 3D open-framework metal sulfates derived from these chains under appropriate conditions. The half-kagome structure of **6** involving mixed-valent Fe is especially interesting as it exhibits ferrimagnetic properties at low temperatures and shows no clear evidence of frustration.

Experimental Section

Synthesis and Initial Characterization

Compounds **1**–**6** were synthesized by employing mild hydro/solvothermal methods. In a typical synthesis of **1**, $ZnCl_2$ (0.136 g) was dissolved in water (3.6 mL) under constant stirring. H_2SO_4 (0.16 mL) and bpy (0.468 g) were added to this solution, and the mixture was stirred for 30 min. The final mixture with molar composition $ZnCl_2$/bpy/H_2SO_4/H_2O 1:2:3:200 was transferred to a 7-mL PTFE-lined acid-digestion bomb and heated at 150 °C for 48 h. The product contained brownish needle-shaped crystals of **1** in 80% yield. For the preparation of **6**, $Fe(NO_3)_3{\cdot}9H_2O$ (0.404 g) was dissolved in ethyleneglycol (eg) (4.6 mL) under constant stirring. Piperazine (pip) (0.3445 g) and sulfuric acid (98%) (0.22 mL) were added to this mixture followed by the addition of HF (40%) (0.36 mL). The resultant mixture with the molar composition $Fe(NO_3)_3{\cdot}9H_2O$/H_2SO_4/pip/eg/HF 1:4:4:8:8 had an initial pH value <2 after stirring for 2 h. The mixture was taken in a 23-mL PTFE-lined acid-digestion bomb and heated at 180 °C for 2 days. After cooling to room temperature, pink rod-shaped crystals of **6** were isolated in 60% yield. The synthetic conditions employed for the preparation of **1**–**6** are listed in Table 5.

Initial characterization of **1**–**6** was carried out by powder X-ray diffraction (PXRD), energy-dispersive analysis of X-rays (EDAX), thermogravimetric analysis (TGA), and IR spectroscopy. Magnetic measurements on powdered samples were performed at temperatures between 2 and 300 K on a vibrating-sample magnetometer using a physical-property

Table 5. Synthetic conditions and analysis of compounds **1**–**6**.

	Starting composition[a]	T [K]	t [h]	pH	M/S[b]	Formula	Yield [%]
1	$ZnCl_2$/H_2SO_4/bpy/H_2O (1:3:2:200)	423	48	2	1:1	$[C_{10}N_2H_{10})][Zn(SO_4)Cl_2]$	80
2	$Mn(OAC)_2$/H_2SO_4/hmda/H_2O/butan-1-ol (1:4:2.5:50:50)	423	72	2	1:2	$C_6N_2H_{18}][Mn(SO_4)_2(H_2O)_2]$	70
3	NiO/H_2SO_4/en/H_2O/eg[c] (1:3:2:50:50)	453	48	2	1:2	$[C_2N_2H_{10}][Ni(SO_4)_2(H_2O)_2]$	50
4	$V(acac)_3$[d]/H_2SO_4/pip/H_2O/eg	453	72	2	1:2	$[C_4N_2H_{12}][V^{III}(OH)(SO_4)_2].H_2O$	60
5	$VOSO_4{\cdot}5H_2O$/H_2SO_4/pip/H_2O/eg/HF (2:3:3:50:100:4)	453	48	2	1:1	$[C_4N_2H_{12}][V^{III}F_3(SO_4)]$	65
6	$Fe(NO_3)_3{\cdot}9H_2O$/H_2SO_4/pip/eg/HF (1:4:4:80:8)	453	48	2	2:1	$[C_4N_2H_{12})][H_3O][Fe^{III}Fe^{II}F_6(SO_4)]$	60

[a] H_2SO_4: 98% (*w*/*w*) in water; HF: 48% (*w*/*w*) in water. [b] The metal to sulfur ratios obtained by EDAX. [c] Ethylene glycol. [d] Vanadium(III) acetyl acetonate.

measurement system (quantum design). PXRD patterns indicated the products to be new materials and monophasic, the patterns being consistent with those generated from single-crystal X-ray diffraction. EDAX gave the expected metal/sulfate ratios of 1:1, 1:2, 1:2, 1:1, 1:2, and 2:1 for **1–6**, respectively.

Infrared spectra of **1–6** showed characteristic bands due to the sulfate ion in the 1100 and 620 cm^{-1} regions, besides bands due to C–H stretching and bending vibrations as well as those due to the amine moiety.[21] A band at around 1020–1040 cm^{-1} in **4** is observed as a result of the V–O–H bending mode. Bands at around 3500 cm^{-1} were found in **4** and **6** due to the presence of water. A band at around 1620–1640 cm^{-1} for **2** and **3** was assigned to coordinated water.

Thermogravimetric analysis of **1–6** was carried out under constant flow of N_2 at a heating rate of 5 °C min^{-1} in the temperature range 30–900 °C. Compound **1** showed a two-step weight loss corresponding to the loss of bpy in the range 200–250 °C (obs = 43.8 %, calcd = 44.1 %) followed by the removal of SO_3 and Cl_2 in the range 400–800 °C (obs = 21.3 %, calcd = 22.6 %).

The PXRD pattern of the sample heated to 900 °C corresponded to ZnO (JCPDS file card 01–1136). In **2**, there was a three-step weight loss corresponding to the loss of water in the range 100–200 °C (obs = 9.3 %, calcd = 8.9 %), the amine molecules at 300 °C (obs = 28.9 %, calcd = 29.3 %), and decomposition of sulfate in the range 400–800 °C (obs = 44 %, calcd = 42.4 %). The PXRD pattern of the sample heated to 900 °C corresponded to Mn_3O_4 (JCPDS file card 08–0017). Compound **3** showed a two-step weight loss at around 100–120 °C corresponding to the loss of water molecules (obs = 11 %, calcd = 10.3 %). The second weight loss in the broad temperature range 200–550 °C is due to the loss of the amine and SO_3 (obs = 59.86 %, calcd = 62.8 %). The PXRD pattern of the sample heated to 900 °C corresponded to NiO (JCPDS file card 22–1189). Compound **4** showed a three-step weight loss corresponding to the loss of water molecules at 150 °C (obs = 5.1 %, calcd = 4.9 %), amine and SO_2 in the range 300–450 °C (obs = 52.4 %, calcd = 50.8 %), and removal of rest of SO_3 in the range 450–800 °C (obs = 19.6 %, calcd = 18.6 %). The PXRD pattern of the sample heated to 900 °C corresponded to V_2O_3 (JCPDS file card 26–0278). Compound **5** showed a sharp two-step weight loss at around 300–400 °C corresponding to the loss of piperazine, HF, and F_2 (obs = 55 %, calcd = 53.4 %) and SO_3 (obs = 22.6 %, calcd = 21.5 %). The PXRD pattern of the sample heated to 900 °C corresponded to V_2O_3 (JCPDS file card 34–0187). Compound **6** revealed a three-step weight loss corresponding to loss of water at 100 °C (obs = 4.7 %, calcd = 4.2 %), amine, HF, and F_2 in the 250–400 °C range (obs = 48.3 %, calcd = 47.4 %) and decomposition of the sulfate in the 400–800 °C range (obs = 11.8 %, calcd = 11.6 %). The powder X-ray diffraction pattern of the decomposed product corresponded to Fe_2O_3 (JCPDS file card 33–0664).

The presence of fluorine atoms in **5** and **6** was confirmed by qualitative analysis, bond valence sum calculations, and also from the absence of electron density near fluorine in the difference Fourier map.

Single-Crystal-Structure Determination

A suitable single crystal of each compound was carefully selected under a polarizing microscope and mounted at the tip of the thin glass fiber by using cyanoacrylate (superglue) adhesive. Single-crystal-structure determination by X-ray diffraction was performed on a Siemens SMART-CCD diffractometer equipped with a normal-focus 2.4-kW sealed-tube X-ray source ($Mo_{K\alpha}$ radiation, $\lambda = 0.71073$ Å) operating at 50 kv and 40 mA. The structure was solved by direct methods using SHELXS-86,[22] which readily revealed all the heavy atom positions (Zn, Mn, Ni, V, Fe, S, Cl) and enabled us to locate the other non-hydrogen (C, N, O, and F) positions from the difference Fourier maps. An empirical absorption correction based on symmetry-equivalent reflections was applied by using SADABS[23]. All the hydrogen positions for compound **1–6** were found in

Table 6. Crystal data and structure refinement parameters for compounds **1–6**.

Parameters	**1**	**2**	**3**	**4**	**5**	**6**
empirical formula	$C_{10}H_{10}Cl_2N_2O_4SZn$	$C_3H_{11}Mn_{0.5}NO_5S$	$C_2H_{14}NiN_2O_{10}S_2$	$C_4H_{15}N_2O_{10}S_2V$	$C_4H_{12}F_3N_2O_4SV$	$C_4H_{15}F_6Fe_2N_2O_5S$
crystal system	triclinic	triclinic	triclinic	monoclinic	triclinic	triclinic
space group	P-1(2)	P-1(2)	P-1(2)	$P2_1/c$ (14)	P-1(2)	P-1(2)
crystal size [mm^3]	0.30×0.15×0.15	0.20×0.16×0.12	0.16×0.12×0.08	0.24× 0.12×0.08	0.18×0.12×0.08	0.21×0.15×0.12
a [Å]	4.912(3)	5.2330(2)	5.1738(7)	9.2964(7)	7.3363(13)	7.2301(9)
b [Å]	8.460(9)	5.77580(10)	7.5094(10)	18.3093(15)	8.5711(14)	9.0548 (11)
c [Å]	17.240(11)	12.9081(5)	7.6163(10)	7.1546(6)	8.5888(14)	9.5967(12)
α [°]	85.07(4)	92.202(2)	82.303(3)	90.00(0)	70.999(3)	95.137(2)
β [°]	88.51(6)	94.435(2)	70.743(2)	98.166(2)	73.464(3)	92.217(2)
γ [°]	80.47(5)	102.481(2)	74.577(3)	90.000(0)	69.909(3)	96.901(2)
V [Å^3]	703.8(2)	379.17(2)	268.95(6)	1205.44(2)	470.40(14)	620.43(13)
Z	2	2	2	4	2	2
formula mass	390.53	200.66	348.98	366.24	292.15	428.94
ρ_{calcd} [g cm^{-3}]	1.843	1.758	2.155	2.018	2.063	2.296
λ ($Mo_{K\alpha}$) [Å]	0.71073	0.71073	0.71073	0.71073	0.71073	0.71073
μ [mm^{-1}]	2.284	1.195	2.242	1.222	1.322	2.604
θ range [°]	1.19–23.28	1.58-23.28	2.82-23.24	2.21-23.27	2.56-23.29	2.13-23.28
total data collected	3030	1562	1115	1727	1985	2583
unique data	2024	1055	759	1001	1985	1769
refinement method	Full-matrix least squares on $\|F^2\|$	Full-matrix least squares on $\|F^2\|$	Full-matrix least squares on $\|F^2\|$	Full-matrix least squares on $\|F^2\|$	Full-matrix least squares on $\|F^2\|$	Full-matrix least squares on $\|F^2\|$
R_{int}	0.0322	0.0301	0.0389	0.0968	0.0417	0.0250
$R[I>2\sigma(I)]$	$R_1 = 0.0467$, $wR_2 = 0.0942$	$R_1 = 0.0473$, $wR_2 = 0.1201$	$R_1 = 0.0377$, $wR_2 = 0.0908$	$R_1 = 0.0752$, $wR_2 = 0.1989$	$R_1 = 0.0608$, $wR_2 = 0.1195$	$R_1 = 0.0546$, $wR_2 = 0.1413$
R (all data)	$R_1 = 0.0738$, $wR_2 = 0.1113$	$R_1 = 0.0531$, $wR_2 = 0.1234$	$R_1 = 0.0434$, $wR_2 = 0.0928$	$R_1 = 0.1219$, $wR_2 = 0.2309$	$R_1 = 0.1081$, $wR_2 = 0.1427$	$R_1 = 0.0702$, $wR_2 = 0.1525$
goodness of fit (S)	1.051	1.005	0.987	0.957	1.055	1.017
largest difference map peak and hole [eÅ]	0.517 and −0.545	0.542 and −0.733	0.583 and −0.730	0.932 and −977	0.546 and −0.595	1.948 and −0.804

[a] $R_1 = \Sigma\,||F_0| - |F_c||/\Sigma\,|F_0|$ [b] $wR_2 = \{[w(F_0^2 - F_c^2)^2]/[w(F_0^2)^2]\}^{1/2}$, $w = 1/[\sigma^2(F_0)^2 + (aP)^2 + bP]$ $P = [F_0^2 + 2F_c^2]/3$ (a = 0.0482, 0.0904, 0.0393, 0.1535, 0.0452, 0.1066 and b = 0, 0, 0, 0, 1.6190, 0 for **1–6**, respectively).

the difference Fourier maps. For the final refinement, hydrogen atom of both the framework as well the amine were placed geometrically and held in the riding mode. The last cycles of refinement included atomic positions; anisotropic thermal parameters for all the non-hydrogen atoms and isotropic thermal parameters for all the hydrogen atoms. Full-matrix least-squares structure refinement against $|F^2|$ was carried out with the SHELXTL-PLUS[24] package of programs. The positions of the fluorine atoms in **5** and **6** were located primarily by looking at their thermal parameters; assignment as oxygen atoms instead of fluorine invariably leads to nonpositive definite values when they are refined by anisotropic displacement parameters. The absence of electron density near the fluorine atom in the difference Fourier map also helped to differentiate fluorine atoms and hydroxy groups in **5** and **6**. Details of the structure determination and final refinements for **1**–**6** are listed in Table 6. Powder X-ray diffraction patterns of **1**–**6** were in good agreement with the simulated patterns based on single-crystal data, indicative of their phase purity.

CCDC-600776–600781 (**1**–**6**, respectively) contains the supplementary crystallographic data for this paper. These data can be obtained free of charge at www.ccdc.cam.ac.uk/conts/retrieving.html (or from the Cambridge Crystallographic Data Centre, 12, Union Road, Cambridge CB2 1EZ, UK; fax: (+44) 1223–336–033; e-mail: deposit@ccdc.cam.ac.uk).

Acknowledgements

We thank Dr. S. K. Pati for useful discussions. J. N. Behera thanks CSIR, India, for a Senior Research Fellowship.

[1] a) D. W. Breck; *Zeolite Molecular Sieves*, Wiley, New York, **1974**; b) W. M. Meier, D. H. Oslen, C. Baerlocher, *Atlas of Zeolite Structure Types*, Elsevier: London, **1996**.

[2] a) A. K. Cheetam, G. Ferey, T. Loiseau, *Angew. Chem.* **1999**, *111*, 3466; *Angew. Chem. Int. Ed.* **1999**, *38*, 3268; b) C. N. R. Rao, S. Natarajan, A. Choudhury, S. Neeraj, A. A. Ayi, *Acc. Chem. Res.* **2001**, *34*, 80.

[3] a) C. N. R. Rao, S. Natarajan, R. Vaidyanathan, *Angew. Chem.* **2004**, *116*, 1490; *Angew. Chem. Int. Ed.* **2004**, *43*, 1466; b) C. Livage, C. Egger, G. Ferey, *Chem. Mater.* **1999**, *11*, 1546; c) T. M. Reinke, M. Eddaoudi, M. O′ Keeffe, O. M. Yaghi, *Angew. Chem.* **1999**, *111*, 2712; *Angew. Chem. Int. Ed.* **1999**, *38*, 2590; d) H. Li, M. Eddaoudi, T. L. Groy, O. M. Yaghi, *J. Am. Chem. Soc.* **1998**, *120*, 8571.

[4] a) J. N. Behera, K. V. Gopalkrishnan, C. N. R. Rao, *Inorg. Chem.* **2004**, *43*, 2636; b) G. Paul, A. Choudhury, R. Nagarajan, C. N. R. Rao, *Inorg. Chem.* **2003**, *42*, 2004; c) G. Paul, A. Choudhury, C. N. R. Rao, *Chem. Mater.* **2003**, *15*, 1174; d) G. Paul, A. Choudhury, C. N. R. Rao, *J. Chem Soc. Dalton Trans.* **2002**, *20*, 3859; e) J. N. Behera, G. Paul, A. Choudhury, C. N. R. Rao, *Chem. Commun.* **2004**, 456; f) C. N. R. Rao, E. V. Sampathkumaran, R. Nagarajan, G. Paul, J. N. Behera, A. Choudhury, *Chem. Mater.* **2004**, *16*, 1441; g) G. Paul, A. Choudhury, C. N. R. Rao, *Chem. Commun.* **2002**, 1904; h) A. Choudhury, J. Krishnamoorthy, C. N. R. Rao, *Chem. Commun.* **2001**, 2610; i) C. N. Morimoto, E. C. Lingafelter, *Acta Crystallogr. Sect. B* **1970**, *26*, 335; j) G. Paul, A. Choudhury, E. V. Sampathakumaran, C. N. R. Rao, *Angew. Chem.* **2002**, *114*, 4473; *Angew. Chem. Int. Ed.* **2002**, *41*, 4297.

[5] a) A. Choudhury, D. Udayakumar, C. N. R. Rao, *Angew. Chem.* **2002**, *114*, 2306; *Angew. Chem. Int. Ed.* **2002**, *41*, 158; b) D. Udayakumar, C. N. R. Rao, *J. Mater. Chem.* **2003**, *13*, 1635; c) W. T. A. Harrison, M. L. F. Phillips, J. Stanchfield, T. M. Nenoff, *Angew. Chem.* **2000**, *112*, 3966; Angew. Chem. Int. Ed. **2000**, 39, 3808; d) I. Pasha, C. N. R. Rao, *Inorg. Chem.* **2003**, *42*, 409; e) I. Pasha, A. Choudhury, C. N. R. Rao, *Solid State Sci.* **2003**, *5*, 257; f) F. Millange, C. Serre, T. Cabourdin, J. Marrot, G. Ferey, *Solid State Sci.* **2004**, *6*, 229; g) Z. Dai, Z. Shi, G. Li, X. Chen, X. Lu, Y. Xu, S. Feng, *J. Solid State Chem.* **2003**, *172*, 205.

[6] a) J. N. Behera, A. A. Ayi, C. N. R. Rao, *Chem. Commun.* **2004**, 968; b) I. Pasha, A. Choudhury, C. N. R. Rao, *J. Solid State Chem.* **2003**, *174*, 386; c) M.-L. Feng, J.-G. Mao, J.-L. Song, *J. Solid State Chem.* **2004**, *177*, 3529; d) D. Udayakumar, M. Dan, C. N. R. Rao, *Eur. J. Inorg. Chem.* **2004**, 1733.

[7] C. N. R. Rao, J. N. Behera, M. Dan, *Chem. Soc. Rev.* **2006**, *35*, 375.

[8] a) A. P. Ramirez, *Annu. Rev. Mater. Sci.* **1994**, *24*, 453; b) J. E. Greedan, *J. Mater. Chem.* **2001**, *11*, 37; c) D. G. Nocera, B. M. Bartlett, D. Grohol, D. Papoutsakis, M. P. Shores, *Chem. Eur. J.* **2004**, *10*, 3850.

[9] J. N. Behera, C. N. R. Rao, *Z. Anorg. Allg. Chem.* **2005**, 631, 3030.

[10] a) F. C. Hawthrone, S. V. Krivovichev, P. C. Burns, *Rev. Mineral. Geochem.* **2000**, *40*, 1; b) F. C. Hawthrone, S. V. Krivovichev, P. C. Burns, *Rev. Mineral. Geochem.* **2000**, *40*, 55.

[11] M. Fleck, U. Kolitsch, B. Hertweck, G. Geister, M. Wildner, M. Prem, A. Wohlschlager, *Z. Kristallogr.* **2002**, *217*, 1.

[12] M. Fleck, U. Kolitsch, B. Hertweck, *Z. Kristallogr.* **2002**, *217*, 435.

[13] a) Z. Bircsak, W. T. A. Harrison, *Inorg. Chem.* **1998**, *37*, 3204; b) E. Alda, B. Bazan, J. L. Mesa, J. L. Pizarro, M. I. Arriortua, T. Rojo, *J. Solid State Chem.* **2003**, *173*, 101.

[14] L. Fafani, A. Nunzi, P. F. Zanazzi, *Am. Mineral.* **1971**, *56*, 751.

[15] a) N. E. Brese, M. O′Keefee, *Acta Crystallogr. Sect. B* **1991**, *47*, 192; b) I. D. Brown, D. Altermatt, *Acta Crystallogr. Sect. B* **1985**, *41*, 244.

[16] a) A. S. Wills, A. Harrison, *J. Chem. Soc. Faraday Trans.* **1996**, *92*, 2161; b) T. Inami, M. Nishiyama, S. Maegawa, Y. Oka, *Phys. Rev. B* **2000**, *61*, 12181; c) J. N. Reimers, A. J. Berlinsky, *Phys. Rev. B* **1993**, *48*, 9539; d) J. Frunzke, T. Hansen, A. Harrison, J. S. Lord, G. S. Oakley, D. Visser, A. S. Wills, *J. Mater. Chem.* **2001**, *11*, 179; e) A. S. Wills, A. Harrison, C. Ritter, R. I. Smith, *Phys. Rev. B* **2000**, *61*, 6156; f) E. A. Earle, A. P. Ramirez, R. J. Cava, *Phys. B* **1999**, *262*, 199; g) S.-H. Lee, C. Broholm, M. F. Collins, L. Heller, A. P. Ramirez, Ch. Kloc, E. Bucher, R. W. Erwin, N. Lacevic, *Phys. Rev. B* **1997**, *56*, 8091.

[17] C. N. R. Rao, G. Paul, A. Choudhury, E. V. Sampathakumaran, A. K. Raychaudhuri, S. Ramasesha, I. Rudra, *Phys. Rev. B* **2003**, *67*, 134425.

[18] a) S. K. Pati, S. Ramasasha, D. Sen, *Phys. Rev. B* **1997**, *55*, 8894; b) S. K. Pati, *Phys. Rev. B* **2003**, *67*, 184411; c) V. R. Chandra, D. Sen, N. B. Ivanov, J. Richter, *Phys. Rev. B* **2004**, *69*, 214406.

[19] S. K. Pati, C. N. R. Rao, *J. Chem. Phys.* **2005**, *123*, 234703.

[20] B. M. Bartlett, D. G. Nocera, *J. Am. Chem. Soc.* **2005**, *127*, 8985.

[21] K. Nakamoto, *Infrared and Raman Spectra of Inorganic and Coordination Compounds*, Wiley Interscience, New York, **1978**.

[22] G. M. Sheldrick, *SHELXS-86 Program for Crystal Structure Determination*, University of Göttingen, Göttingen, Germany, **1986**.

[23] G. M. Sheldrick, *SADABS*: *Siemens Area Detector Absorption Correction Program*, University of Göttingen, Göttingen, Germany, **1994**.

[24] G. M. Sheldrick, *SHELXTL-PLUS Program for Crystal Structure Solution and Refinement,* University of Göttingen, Göttingen, Germany, **1993**.

Received: March 20, 2006
Revised: August 18, 2006

